



Beam shaping to enhance zero group velocity Lamb mode generation in a composite plate and nondestructive testing application

Frédéric Faëse, Samuel Raetz, Nikolay Chigarev, Charfeddine Mechri, James Blondeau, Benjamin Campagne, Vitali Goussev, Vincent Tournat

► To cite this version:

Frédéric Faëse, Samuel Raetz, Nikolay Chigarev, Charfeddine Mechri, James Blondeau, et al.. Beam shaping to enhance zero group velocity Lamb mode generation in a composite plate and nondestructive testing application. NDT & E International, 2017, 85, pp.13 - 19. 10.1016/j.ndteint.2016.09.003 . hal-01889431v1

HAL Id: hal-01889431

<https://univ-lemans.hal.science/hal-01889431v1>

Submitted on 6 Oct 2018 (v1), last revised 27 Apr 2019 (v2)

HAL is a multi-disciplinary open access archive for the deposit and dissemination of scientific research documents, whether they are published or not. The documents may come from teaching and research institutions in France or abroad, or from public or private research centers.

L'archive ouverte pluridisciplinaire **HAL**, est destinée au dépôt et à la diffusion de documents scientifiques de niveau recherche, publiés ou non, émanant des établissements d'enseignement et de recherche français ou étrangers, des laboratoires publics ou privés.

1 Beam shaping to enhance zero group velocity Lamb
2 mode generation in a composite plate and
3 nondestructive testing application

4 Frédéric Faëse^{a,b}, Samuel Raetz^{b,*}, Nikolay Chigarev^b, Charfeddine Mechri^b,
5 James Blondeau^b, Benjamin Campagne^c, Vitalyi E. Gusev^b, Vincent
6 Tournat^{b,1,**}

7 ^a*IRT Jules Verne, Chemin du Chaffault, 44340 BOUGUENNAIS - France*

8 ^b*Université du Maine, CNRS, LAUM UMR 6613, Av. O. Messiaen, 72085 LE MANS*
9 *Cedex 9 - France*

10 ^c*Airbus Group Innovations, Chemin du Chaffault, 44340 BOUGUENNAIS - France*

11 **Abstract**

Zero group velocity (ZGV) Lamb modes have already shown their potential in nondestructive testing applications as they are sensitive to the sample structural characteristics. In this paper, we first consider an aluminum sample to validate a method based on the beam shaping of the generation laser. This method is proven to enhance ZGV Lamb modes in aluminum, and then advantageously applied to a composite material plate. Finally, based on the proposed method, scanning the sample over healthy and flawed zones demonstrates the ability to detect subsurface flaws.

12 *Keywords:* Laser ultrasonics, Composite materials, Zero Group Velocity
13 Lamb modes, NDT

*Corresponding author

**Principal corresponding author

Email addresses: samuel.raetz@univ-lemans.fr (Samuel Raetz),
vincent.tournat@univ-lemans.fr (Vincent Tournat)

¹Currently at: John A. Paulson School of Engineering and Applied Science, Harvard University, Cambridge, MA 02138, USA

Preprint submitted to NDT&E International

May 3, 2016

14 1. Introduction

15 Laser ultrasonics is a more and more widespread nondestructive testing
16 method as it shows specific advantages compared to conventional ultrasonic
17 methods based on transducers or EMATs. Particularly, it has a high spatial
18 resolution, a large bandwidth, and it is non-contact [1]. Thanks to these fea-
19 tures, laser ultrasonic techniques allow characterizing the mechanical prop-
20 erties and/or evaluating the structural health of materials, even where the
21 tested samples present complex geometry and/or are subjected to extreme
22 conditions such as high temperatures [2]. Up to now, applications of laser
23 ultrasonic methods have already proved their potential in nondestructive
24 testing of composite materials. They have been implemented successfully to
25 detect delaminations with a propagative Lamb waves analysis [3] or by laser
26 tapping [4]. They have also the ability to detect fiber breakage or matrix
27 cracking via the scanning laser source technique [5] or even porosity thanks
28 to an ultrasonic spectroscopy method [6].

29 Guided waves have been used in composite samples testing and evalua-
30 tion because of their ability to detect a defect at a long propagation distance
31 from the acoustic source position. Yet, the defect position is hard to pre-
32 cisely estimate at a single interface at any position through the laminate [3].
33 As well, a lateral position estimation needs methods with a transducer raster
34 scan like the SAFT method [7] or transducer arrays like the topological imag-
35 ing technique [8]. For ten years, some specific non-propagative Lamb modes
36 called zero group velocity (ZGV) Lamb modes have been studied and already
37 applied to defect detection. Considering a dispersion curve representing the
38 angular frequency ω as a function of the wave number k , these specific modes

are located in the points of a non-zero wave number k where the slope of this curve is horizontal, i.e. $d\omega/dk = 0$. Characterized by a high quality factor, these modes are used for instance to measure thickness variations due to corrosion, to detect disbonding or to determine elastic constants [9, 10]. A method based on the ZGV Lamb modes offers the advantages of being local and having a spatial resolution of the order of the plate thickness [10]. One objective of this article is to report on the effect of a flaw in a composite plate on ZGV Lamb modes.

The challenges to address when generating ZGV Lamb modes in composite plates are numerous. Firstly, the composite plates usually have a low damage threshold. For instance, the sample used in this paper showed fiber whitening at about 5 MW.cm^{-2} with a 1064 nm-wavelength laser, whereas the threshold for aluminum in the same experimental conditions is about 50 MW.cm^{-2} [11]. Secondly, as composite surfaces are matt and diffusive for light, ultrasonic waves are hardly detectable using non-contact optical techniques. Thirdly, quality factors of ZGV Lamb modes are strongly reduced because of the resin viscoelasticity leading to a strong sound attenuation in composite plates. Note that ZGV Lamb modes could even not exist, regarding the anisotropic mechanical properties of the material; nevertheless, this is out of the focus of this paper.

In this work, elastic waves are generated in an aluminum plate or a composite plate by a pulsed laser and detected using an interferometer. By varying the focusing of the pump laser beam, it is possible to favor the generation of either the propagating modes or the ZGV modes in the plate. Especially, considering a circular laser spot as the thermoelastic source, ZGV

Lamb modes are efficiently excited when the spot radius is about the plate thickness [12]. It is first shown that ZGV Lamb modes can be enhanced or reduced in an aluminum plate thanks to a specific beam shaping of the generation laser [13–15]. Then, the same method is advantageously applied to the healthy zone of a composite plate. Finally, a damaged region of the same composite plate is considered and the influences of the flaw on the ZGV Lamb modes are analyzed. Before going into details, the mechanical properties of the tested sample and the experimental setups are introduced.

2. Mechanical properties of the tested sample and experimental setups

Since it is here proposed to study the influence of flaws on ZGV Lamb modes in a plate of composite material by using a beam-shaping mask to selectively generate a specific ZGV mode, it is important to know the mechanical properties of the tested material in order to design the beam-shaping mask. We will show that the optimal geometrical properties of the beam-shaping mask for a particular ZGV mode generation depend on the ZGV wavelength in the sample. In the framework of industrial nondestructive testing (NDT), mechanical properties of the composite materials are already well characterized. Hence, the wavelengths of the ZGV modes that can be generated in the sample can be known. Here the mechanical properties of the composite sample were first characterized in order to determine an interesting ZGV mode and then to make the appropriate beam-shaping mask.

In order to predict the dispersion curve of the composite plate, both the density and the elastic constants have to be determined. First, the volumetric mass density of the composite sample has been estimated thanks to

89 Archimedes principle to be $\rho_{comp} \approx 1540 \text{ kg.m}^{-3}$. Second, the elastic con-
 90 stants have been determined thanks to a method explained in Refs. [16]
 91 and [17]. Based on appropriate A-scans, plane wavefronts are synthesized
 92 by summing the signals with suitable delays. By changing the synthesized
 93 propagation angle, quasi-longitudinal and quasi-transversal time of flights are
 94 semi-automatically recorded. Finally, the theoretical slowness curve that fits
 95 the experimental one is determined, thanks to a minimization method. This
 96 leads to the following estimation of the elastic constants: $C_{11} = 13.4 \text{ GPa}$,
 97 $C_{12} = 3.00 \text{ GPa}$, $C_{22} = 21.36 \text{ GPa}$, and $C_{55} = 3.64 \text{ GPa}$. Note that these
 98 constants have been obtained by assuming that the composite plate is trans-
 99 versely isotropic relative to an axis normal to the surface. Finally, from the
 100 measured plate thickness, $d_{comp} \approx 3.2 \text{ mm}$, the wavelength of the first ZGV
 101 Lamb mode in the composite plate can be estimated with a precision that is
 102 sufficient for the method we propose: $\lambda_{ZGV}^{comp} \approx 15.3 \text{ mm}$.

103 Due to the low damage threshold of composite materials, the choice has
 104 been done to experimentally use an extended line source instead of a circular
 105 spot, in order to lower the source power density on the sample while keeping
 106 sufficiently large displacement amplitude. Theoretically, using an infinitely
 107 long and thin thermoelastic line source, the amplitude of the surface displace-
 108 ment due to a ZGV Lamb mode as a function of the distance from the line
 109 source is a pure cosine function, since it results from the interference of two
 110 counter-propagative Lamb modes having the same wave number, i.e. of the
 111 form $e^{jk_{ZGV}x}$ and $e^{-jk_{ZGV}x}$. In the case of a finite line source, the amplitude
 112 varies as an intermediate function between the pure cosine function and a
 113 Bessel function [18], the latter standing for the theoretical spatial distribu-

tion of ZGV Lamb modes in the case of a point surface source [12]. In order to selectively generate the first ZGV Lamb mode and to increase the total incident laser power while keeping the power density constant, we propose here to use multiple finite line sources using an appropriate beam-shaping mask. As illustrated in Fig. 1, using the beam-shaping mask allows the generation laser beam to be shaped with periodic slits whose spacing matches the ZGV wavelength, thereby producing a constructive interference of the ZGV Lamb modes generated by each line source.

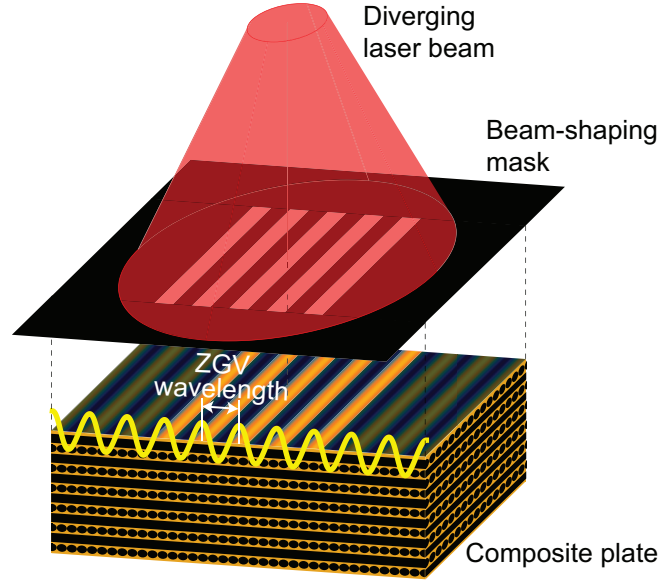


Figure 1: (color online) Illustration of the ZGV Lamb mode generation using a beam-shaping mask. The generation laser beam is shaped with periodic slits whose spacing matches the ZGV wavelength.

In order to analyze the ZGV Lamb mode generation using a shaped laser beam, an experimental setup schematized in Fig. 2 has been implemented. The generation laser is an Nd:YAG laser (Spitlight Compact 400, InnoLas

125 Laser GmbH, Germany) emitting 10 ns pulses at 1064 nm. The pulse energy
126 is limited to a few tens of mJ in order to remain below the damage threshold
127 and to avoid fiber whitening. This limitation of the laser energy is performed
128 using two polarizing beam splitters (PBS) and a half-wave plate ($\lambda/2$) as
129 schematized in Fig. 2. Thanks to a negative lens, the whole beam shaping
130 mask is illuminated by the generation laser. This mask consists of a series
131 of transparent and opaque patterns (Fig. 1) printed on transparency films
132 by a laser printer. Two identical masks are placed one after the other in
133 the close vicinity of the plate in order to obtain a sufficient contrast. The
134 normal surface displacement due to ultrasonic waves is detected on the other
135 side of the sample by a two-wave mixing (TWM) interferometer (LU-TWM-
136 ASGA, Tecnar Canada) whose bandwidth ranges from about 1 MHz to 40
137 MHz [19]. Note that the bandpass spectrum of the interferometer filter is
138 smooth and still allows to detect displacement with frequency component
139 down to about 300 kHz. The TWM is using a CW Nd:YAG laser, the beam
140 of which is guided through an optical fiber to the TWM head including a
141 neutral density filter and the focusing/collecting lens. The TWM head is
142 mounted on a motorized linear stage so that the detection point is scannable
143 over the sample. A second motorized linear stage can also be used to scan
144 the sample in front of fixed generation pattern and detection point. Since
145 generation and detection of elastic waves are on opposite sides, this setup is
146 referred to as the transmission setup in the following.

147 A second setup has been used in this study, with generation and detection
148 on the same side, which is referred to as the reflection setup in the following.
149 It is identical to the transmission setup, except that both generation laser

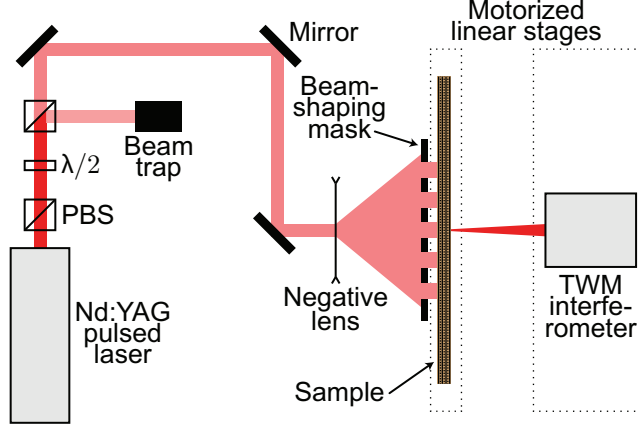


Figure 2: (color online) Schematics of the experimental transmission setup.

150 beam and TWM laser beam illuminate the same side of the sample, and
 151 that the generation laser beam is frequency doubled in order not to dazzle
 152 the TWM interferometer photodiode that is sensitive to 1064 nm radiation.
 153 This setup can particularly be useful for a robot inspection and can give
 154 additional information for a flaw characterization as it will be discussed in the
 155 following: where the transmission setup detects a flaw without information
 156 on its in-depth position, we will see that the reflection setup is able to give
 157 information on the flaw position with respect to the depth.

158 Before applying the proposed method to the detection of a flaw in a
 159 composite plate, it is first proposed to focus on the interest of using a beam-
 160 shaping mask to enhance the ZGV Lamb modes in two samples: first, an
 161 aluminum plate for trivial evidence, and then a composite plate.

3. ZGV Lamb modes enhancement in aluminum and composite plates

In order to validate preliminary results obtained with the transmission setup schematized in Fig. 2, Fig. 3 presents the experimental results obtained in an 4.1 mm-thick aluminum plate using a single thermoelastic line source of dimensions 4.1 x 20 mm². Figs. 3(a)-(b) are slightly saturated in order to improve readability.

The time domain B-scan [Fig. 3(a)] represents the normal surface displacement amplitude as a function of time and the TWM head position. The signals have been registered over 200 μ s with the TWM head position ranging from -50 mm to +50 mm with a 0.5 mm step. Two different kinds of modes are visible: (i) the propagating modes starting at the origin in time and space, and (ii) the ZGV Lamb modes that are visible in time after the propagating modes. The ZGV modes are evidenced by a succession of maxima and minima in time and space, typical of the single frequency and the interferential nature of the ZGV modes.

The frequency domain B-scan [Fig. 3(b)] represents the spectral amplitude module of each A-scan constituting the time domain B-scan as a function of the TWM head position. Each spectrum constituting the frequency domain B-scan has been calculated over the whole corresponding A-scan. At the first, i.e. lowest, expected ZGV Lamb mode frequency, $f_{ZGV}^{Al} \approx 694$ kHz, there is a maxima and minima succession in space that is typical of ZGV Lamb modes obtained with a thermoelastic line source. When zooming at the ZGV frequency [Fig. 3(c)], the first ZGV peak amplitude as a function of the TWM head position (solid) shows the expected theoretical shape

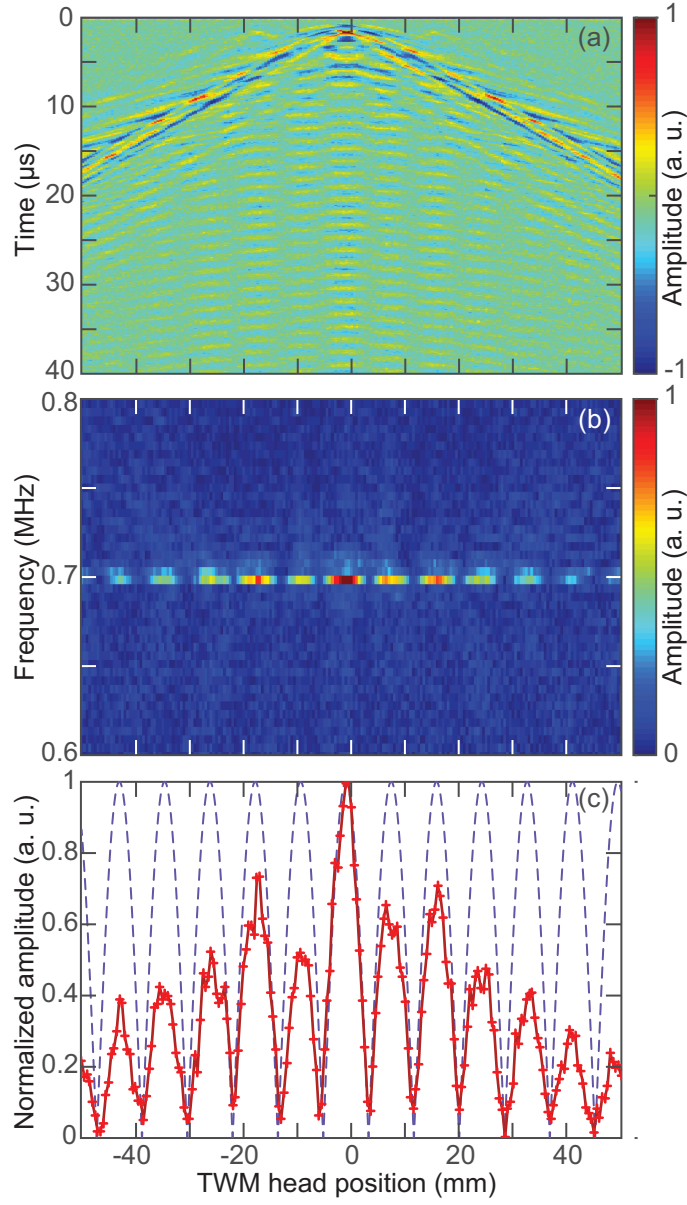


Figure 3: (color online) The thermoelastic source is a line $4.1 \times 20 \text{ mm}^2$: (a) time domain and (b) frequency domain B-scans as a function of the TWM head position. (c) First ZGV peak amplitude vs. TWM head position: experimental (solid) and theoretical (dashed) curves.

187 (dashed), especially regarding the minima. As expected theoretically, the
 188 amplitude of the experimental curve decays with the distance from the line
 189 source position because of the line source finite dimensions.

190 It is now proposed to compare this result obtained with a single line
 191 source to the results obtained with a shaped source composed of lines spaced
 192 by either λ_{ZGV}^{Al} or $\lambda_{ZGV}^{Al}/2$. Figure 4 presents the amplitude of the first ZGV
 193 peak as a function of the TWM head position when the thermoelastic source
 194 is made of: a single line (solid), multiple lines spaced by λ_{ZGV}^{Al} (dashed),
 195 and multiple lines spaced by $\lambda_{ZGV}^{Al}/2$ (dash-dotted). The Frobenius norm
 196 (Euclidian norm) of each normal displacement field is used to normalize each
 197 corresponding curve in Fig. 4, in order for the changes in the absorbed laser
 198 power between the different cases to be compensated.

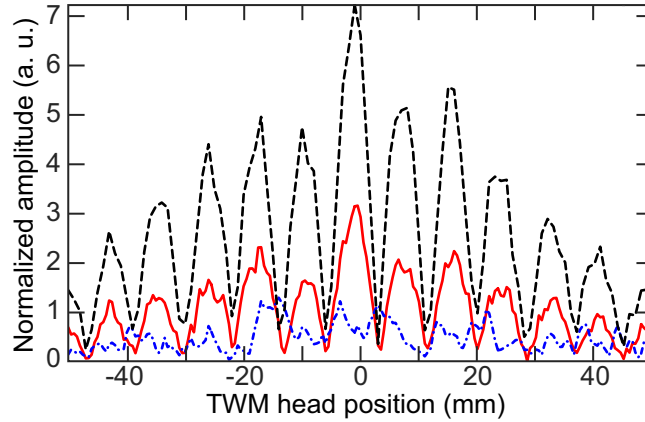


Figure 4: (color online) Normalized first ZGV peak amplitude vs. TWM head position when the thermoelastic source is a single line (solid), multiple lines spaced by λ_{ZGV}^{Al} (dashed) and multiple lines spaced by $\lambda_{ZGV}^{Al}/2$ (dash-dotted).

199 When the lines are spaced by λ_{ZGV}^{Al} , the ZGV Lamb modes are enhanced:
 200 they interfere constructively. On the contrary, when the lines are spaced

201 by $\lambda_{ZGV}^{Al}/2$, the ZGV Lamb mode amplitudes are reduced: they interfere
 202 destructively. As expected, a mask consisting of slits spaced by the ZGV
 203 wavelength enhances the ZGV Lamb modes generation in aluminum com-
 204 pared to a mask consisting of a single slit. The interest of this beam-shaping
 205 method being demonstrated in a metal plate, it is now examined in the more
 206 challenging case of a composite plate.

207 The beam-shaping mask used with the composite plate consists of three
 208 slits spaced by λ_{ZGV}^{comp} . Figures 5(a)-(c) show the experimental results. Fig-
 209 ure 5(a) stands for the time domain B-scan, while Fig. 5(b) shows the fre-
 210 quency domain B-scan. Figures 5(a)-(b) are slightly saturated in order to
 211 improve readability. The amplitude of the first ZGV peak with respect to the
 212 TWM head position obtained for the three-line source (thick line) is com-
 213 pared to the same amplitude obtained with a single line source (thin line) in
 214 Fig. 5(c). The ZGV peak amplitudes in Fig. 5(c) are normalized following
 215 the same method as the one described for aluminum.

216 The time domain B-scan [Fig. 5(a)] highlights the propagating modes
 217 and we slightly see the ZGV Lamb modes. The frequency domain B-scan
 218 [Fig. 5(b)] points out the ZGV Lamb modes at the frequency $f_{ZGV}^{comp} \approx 0.480$ MHz,
 219 which is confirmed by Fig. 5(c). Indeed, as ZGV peaks correspond to energy
 220 peaks, they are expected to be spaced by half the ZGV wavelength, that
 221 is to say that ZGV peaks are expected to be located in the middle of each
 222 illuminated slits as well as centrally located between two adjacent slits. As
 223 Fig. 5(c) shows these peaks on the slits location (under black arrows) and
 224 centrally located between two adjacent slits (under gray arrows), this result
 225 tends to prove the enhancement of the ZGV mode in the composite plate

226 thanks to the proposed beam-shaping mask.

227 In order to obtain Fig. 5(c), the ZGV peak amplitude was measured as the
228 maximum spectral amplitude module between 0.475 MHz and 0.485 MHz.
229 This frequency range can be related to a possible sample thickness variation
230 since the product of the ZGV mode frequency f_{ZGV} by the sample thickness is
231 constant. Hence, the average ZGV frequency $(f_{ZGV})_0$ and the ZGV frequency
232 variation Δf_{ZGV} on the one hand, and the average sample thickness d_0 and
233 the sample thickness variation Δd on the other hand, are related to each
234 other:

$$235 \quad \frac{\Delta d}{d_0} = -\frac{\Delta f_{ZGV}}{(f_{ZGV})_0}. \quad (1)$$

236 The range [0.475-0.485] MHz leads to a thickness variation Δd of about
237 $\pm 33 \mu\text{m}$. This sample thickness variation is very small and it is consistent
238 with the precision of the sample fabrication process.

239 As the beam-shaping method is validated to enhance ZGV Lamb modes
240 in the composite plate, a suitable mask with slits spaced by λ_{ZGV} is now
241 used for an NDT application.

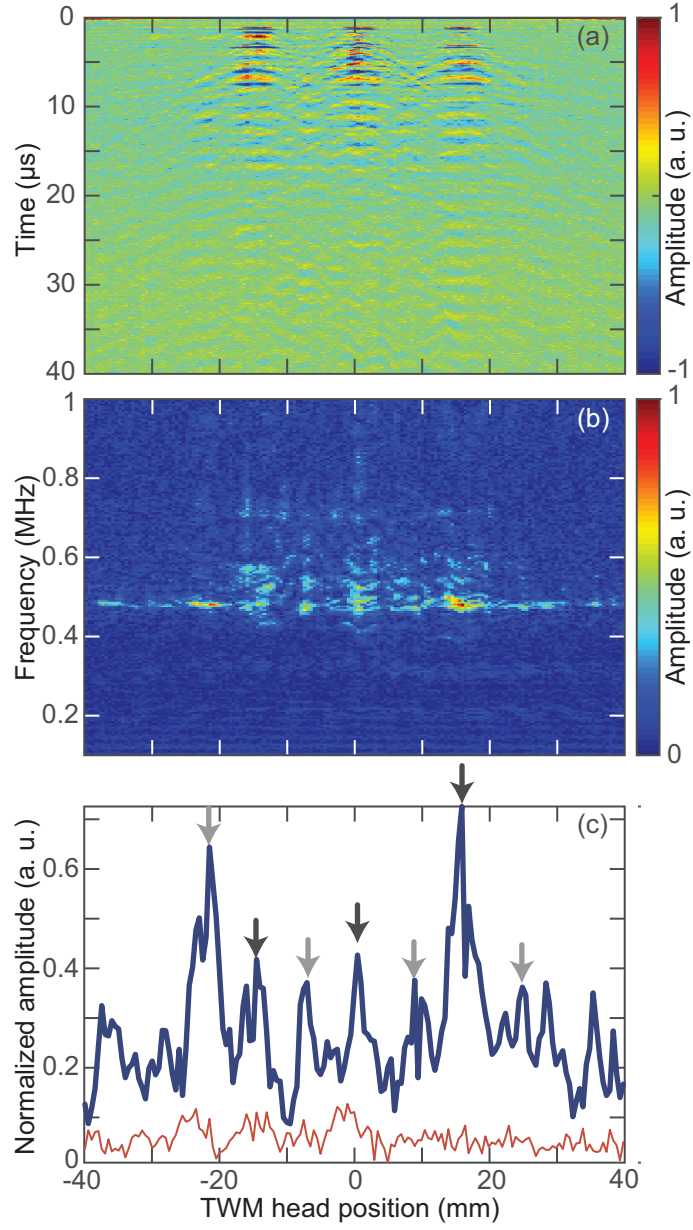


Figure 5: (color online) Results obtained in the composite plate with a thermoelastic source made of three lines: (a) time domain and (b) frequency domain B-scans vs. TWM head position. (c) Normalized amplitude of the first ZGV peak vs. TWM head position (thick line) compared with the result obtained with a single line source (thin line).

242 4. NDT application in a composite plate

243 The reflection setup described in Sec. 2 is now used to scan the composite
244 plate in front of both spatially fixed Nd:YAG frequency doubled laser beam
245 and TWM interferometer beam, the latter being focused to a point in the
246 middle of the beam shaping mask (middle line). As quickly explained in
247 Sec. 2, the choice of using a reflection setup instead of the so-far used trans-
248 mission setup is twofold: (i) this is closer to industrial applicability, and (ii)
249 the flaw in the tested sample is such that, at the flaw location, there is no
250 direct transmission of the elastic waves through the flaw, making the lateral
251 detection of the flaw easy but not the in-depth location. We will see that
252 using a reflection setup can lead to this in-depth characterization of the flaw.

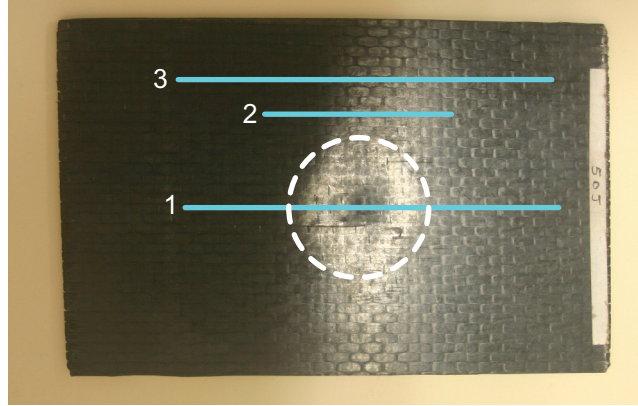


Figure 6: (color online) Composite sample and representation of the scan lines (solid). Dashed white line circle: maximum size of the flaw observed optically.

253 The composite sample presented in Fig. 6 has been impacted by a 50 J
254 centered shock. The 50 J shock was obtained thanks to the drop of a hemi-
255 spherical mass with a diameter of 25 mm. The sample was clamped on a
256 bearing having a 40 mm-diameter hole, centered with respect to the drop

257 mass axis. The first scan line (line 1) crosses the impact whereas the second
 258 scan line (line 2) is near the impact location and the third scan line (line 3) is
 259 far from the impact location. Regarding line 3, note that the thermoelastic
 260 line sources are at least 5 mm away from both the plate edge and the impact
 261 location, whatever the plate position during the scan.

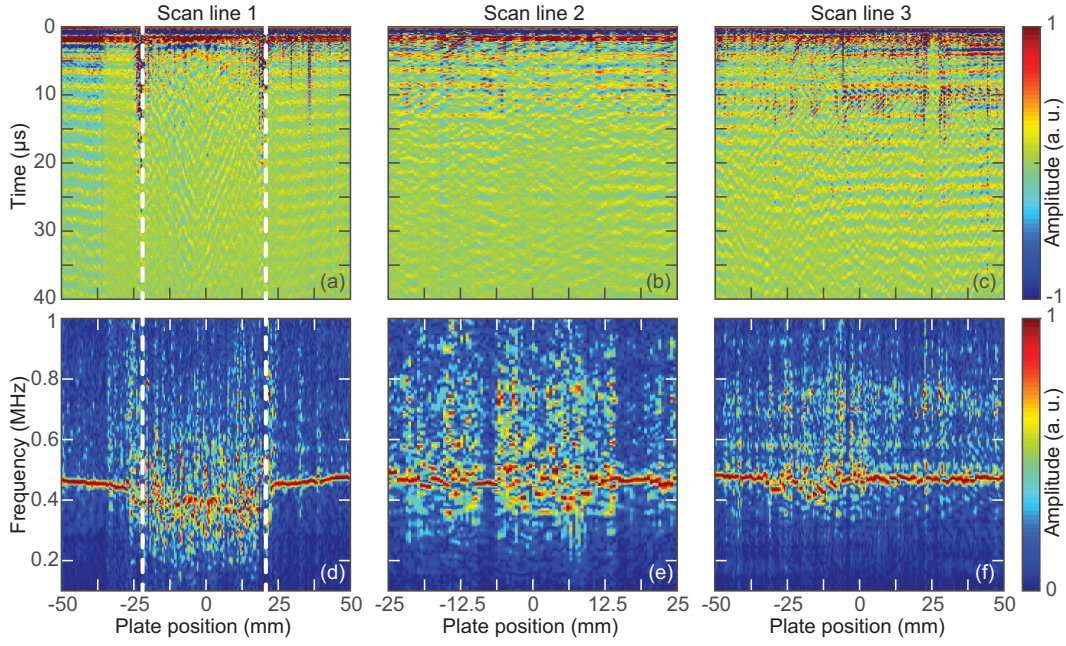


Figure 7: (color online) Time domain B-scans of the composite plate when the scan line is: line 1 across the impact location (a), line 2 near the impact location (b), and line 3 far from the impact location (c). The related frequency domain B-scans obtained with a Hann time window (respectively d, e and f). Dashed white lines: maximum dimension of the flaw observed optically.

262 The time domain B-scan signals have been registered over $200 \mu\text{s}$ with
 263 the plate position ranging from -50 mm to $+50 \text{ mm}$ [Fig. 7(a) and Fig. 7(c)]
 264 or from -25 mm to $+25 \text{ mm}$ [Fig. 7(b)] with a 0.5 mm step. Each A-scan for
 265 a given plate position is numerically post-processed in order to have a zero

mean value over the useful signal duration, i.e. from $10\ \mu\text{s}$ to $100\ \mu\text{s}$. The frequency domain B-scans have then been calculated over the whole time domain signals filtered by a Hann time window ranging from $0\ \mu\text{s}$ to $100\ \mu\text{s}$ in order to emphasize the ZGV Lamb modes. The spectrum amplitude for a given plate position is normalized to its maximum.

In Fig. 7(a), the time domain B-scan across the impact location highlights the impact edges marked by the dashed white lines (cf. also Fig. 6). Moreover, regular successions of maxima and minima in time, representative of ZGV oscillations, can be observed outside of the impact location (in a healthy zone) whereas the signal appears disturbed inside the impact location. The time domain B-scans near the impact location and far from the impact location [Fig. 7(b) and Fig. 7(c), respectively] show minor changes with the plate position and no flaw is clearly evidenced.

The frequency domain B-scan across the impact location [Fig. 7(d)] also clearly highlights the impact as only the ZGV frequency is visible outside the impact location whereas on the impact location the dominant frequency components are spread out over the range $\sim 200 - 800\ \text{kHz}$ and show quick variations in space. Let us also notice that the ZGV frequency decreases almost linearly when the signal measurement gets closer to the impact. As the product f_{ZGV} by the thickness is constant, this shows that either the plate thickness increases with the impact vicinity (the 50 J impact has lead to a bulge at the vicinity of the impact) or the elastic moduli diminish. The frequency domain B-scan near the impact location [Fig. 7(e)] also shows changing multiple frequency components between $-5\ \text{mm}$ and $+15\ \text{mm}$ that could be due to the impact vicinity. Moreover, farther from the impact

location, i.e. between -25 mm and -10 mm, multiple frequency components also appear whereas this zone should be healthy. The frequency domain B-scan far from the impact location [Fig. 7(f)] shows that the main frequency component is the ZGV frequency below -30 mm and above 0 mm; these zones can thus be considered as quasi-healthy zones. On the contrary, between -30 mm and 0 mm, a hidden flaw is detected. This confirms the previous result [Fig. 7(e)] highlighting a flaw on a zone that should be healthy.

These results have been compared to the composite plate inspection obtained with a system called LUCIE, the technical specifications of which are gathered in Ref. [20]. Note that the minimum laser fluence delivered by the pump laser (CO_2 , 270 mJ, 100 ns) in the LUCIE system is 1.5 MW.cm^{-2} , which is below the damage threshold of the composite. Figure 8 represents the C-scan inspection of the composite plate consisting in measuring the ratio of the second ultrasonic echo amplitude to the first ultrasonic echo amplitude as a function of the position on the plate. Note that the ratio can be done after filtering the collected raw data with a selective band-pass filter. LUCIE's data post-processing may also give an image (not shown in this paper) of the time of flight difference between the first and the second detected acoustic echo, although this image is not precise for in-depth localization of defects close to the surface. The presented scan (Fig. 8) shows two major results. First, the 50 J impact is very well identified by the centered zone that shows the lowest value. Second, on the healthy zone scanned previously (cf. line 3 in Fig. 6), the ratio has either values in $[1.95\text{-}3.15]$ % that should be indicative of a real healthy zone or weak values lower than 1.7 % that are indicative of a flaw. This last result confirms the presence of the hidden

316 flaw detected previously along the scan line 3 by the method proposed by
 317 the authors.

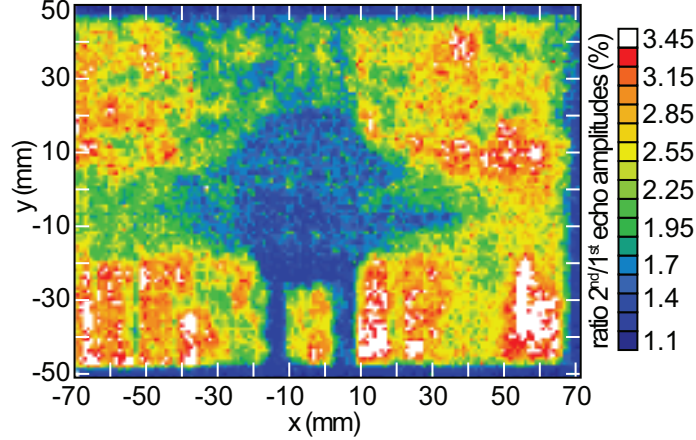


Figure 8: (color online) C-scan inspection of the composite plate obtained with the LUCIE system: ratio of the second ultrasonic echo amplitude to the first ultrasonic echo amplitude

318 Using the experimental transmission setup, a supplementary scan has
 319 been done along the scan line 1, the results of which is not presented in
 320 this paper. The observation is that, at the flaw location, no elastic wave is
 321 directly transmitted. This observation probably means that the 50 J impact
 322 produced a delamination inside the composite plate.

323 Let us consider that the impact produced a delamination inside the com-
 324 posite plate, hence splitting the plate into a minimum of two thinner plates
 325 one above the other. If we assume that laser generated ultrasonic waves
 326 interact only with the top plate, several mechanisms can explain why the
 327 frequency domain B-scans show multiple frequency components on the de-
 328 lamination location. A given frequency component different from the ZGV
 329 mode frequency of the plate can be due to a membrane resonance effect [21]

or to a local defect resonance [22]. It could even be due to another ZGV mode frequency associated to a smaller thickness than the one of the plate. A flaw resonance frequency f_r can be estimated by assuming a circular clamped membrane:

$$f_r = \frac{1.88h}{d^2} \sqrt{\frac{E}{\rho(1-\nu^2)}}, \quad (2)$$

where h and d are the flaw depth and diameter respectively, and E , ρ and ν are the sample Young's modulus, density and Poisson ratio respectively.

If we assume the following typical values: $h = 100 \mu\text{m}$ (a ply thickness), $d = 1.3 \text{ mm}$, $E = 20 \text{ GPa}$, $\rho = 1540 \text{ kg/m}^3$ and $\nu = 0.2$, this leads to a typical value of flaw resonance frequency $f_r \simeq 0.41 \text{ MHz}$, which is in good agreement with the frequency values observed in the frequency domain B-scans in Fig. 7. This estimate suggests that a better knowledge of either the flaw geometry or the local mechanical material properties is necessary to develop a realistic model in relation to our experimental results. This could lead in the future to quantitative estimates of defect parameters relevant for the structural health assessment of composite structures.

5. Conclusion

We have presented a method enabling ZGV Lamb modes enhancement thanks to the beam shaping of the generation laser, making use of a mask with slits spaced by the ZGV wavelength. First, ZGV Lamb modes have been analyzed in an aluminum plate to validate the possibility to enhance or reduce their amplitude depending on the thermoelastic line sources spacing. It has been shown that ZGV Lamb modes interfere constructively when the line sources spacing equals the ZGV wavelength whereas they interfere

354 destructively when the spacing is halved.

355 After the thorough characterization of a composite plate that resulted
356 in the ZGV wavelength determination, the beam-shaping method has been
357 applied to the composite sample. Experimental results demonstrate a ZGV
358 Lamb mode enhancement, hence validating the beam-shaping method also
359 in the case of a composite sample. Finally, by scanning over the sample,
360 the measured signal frequency content near the ZGV frequency has proven
361 its ability to distinguish between healthy zones and an impacted zone of a
362 composite plate, and also to detect flaw zones that are not visually detectable.
363 The next step could possibly be to extract quantitative information from the
364 dominant frequencies of the B-scans compared to those predicted by the
365 mechanical models of the defects.

366 6. Acknowledgments

367 This presentation is part of the LUCITA project managed by IRT Jules
368 Verne (French Institute in Research and Technology in Advanced Manu-
369 facturing Technologies for Composite, Metallic and Hybrid Structures). The
370 authors wish to associate the industrial and academic partners of this project:
371 Airbus Group Innovations and STELIA Aerospace; EMN-Subatech and LAUM
372 respectively.

373 References

- 374 [1] J. Cooper, R. A. Crosbie, R. J. Dewhurst, A. D. W. McKie, and S. B.
375 Palmer, Surface acoustic wave interactions with cracks and slots: A
376 noncontacting study using lasers, *IEEE Trans. Ultrason. Ferroelectr.*
377 *Freq. Control.* **33**, 462–470 (1986).

- 378 [2] D. W. Schindel, D. A. Hutchins, S. T. Smith, and B. Farahbakhsh,
379 Hightemperature pulsed photoacoustic studies of surface waves on solids,
380 *J. Acoust. Soc. Am.* **95**, 2517–2524 (1994).
- 381 [3] N. Guo and P. Cawley, The interaction of Lamb waves with delamina-
382 tions in composite laminates, *J. Acoust. Soc. Am.* **94**, 2240–2246 (1993).
- 383 [4] A. Blouin, C. Néron, B. Campagne, and J.-P. Monchalin, Applications
384 of laser-ultrasonics and laser-tapping to aerospace composite structures.,
385 in *Conference proceedings of 17th WCNDT. Shanghai.*, page 7 (2008).
- 386 [5] P. A. Fomitchov, A. K. Kromin, S. Krishnaswamy, and J. D. Achenbach,
387 Imaging of damage in sandwich composite structures using a scanning
388 laser source technique, *Compos. Part B-Eng.* **35**, 557–562 (2004), marine
389 Composites.
- 390 [6] A. A. Karabutov and N. B. Podymova, Quantitative analysis of the
391 influence of voids and delaminations on acoustic attenuation in CFRP
392 composites by the laser-ultrasonic spectroscopy method, *Compos. Part*
393 *B-Eng.* **56**, 238–244 (2014).
- 394 [7] M. Spies and W. Jager, Synthetic aperture focusing for defect recon-
395 struction in anisotropic media, *Ultrasonics* **41**, 125–131 (2003).
- 396 [8] S. Rodriguez, M. Castaings, M. Deschamps, and E. Ducasse, Topological
397 imaging of defects in anisotropic plates, in V. Le Cam, L. Mevel, and
398 F. Schoefs, editors, *EWSHM - 7th European Workshop on Structural*
399 *Health Monitoring*, pages 1155–1162 (2014).

- 400 [9] D. Clorennec, C. Prada, and D. Royer, Local and noncontact measure-
401 ments of bulk acoustic wave velocities in thin isotropic plates and shells
402 using zero group velocity Lamb modes, *J. Appl. Phys.* **101**, 034908
403 (2007).
- 404 [10] D. Clorennec, C. Prada, and D. Royer, Laser ultrasonic inspection of
405 plates using zero-group velocity Lamb modes, *IEEE Trans. Ultrason.*
406 *Ferroelectr. Freq. Control.* **57**, 1125–1132 (2010).
- 407 [11] J. F. Ready, in J. F. Ready, editor, *Effects of High-Power Laser Radia-*
408 *tion*, chapter 3, pages 67–125, Academic Press (1971).
- 409 [12] O. Balogun, T. W. Murray, and C. Prada, Simulation and measure-
410 ment of the optical excitation of the S_1 zero group velocity Lamb wave
411 resonance in plates, *J. Appl. Phys.* **102**, 064914 (2007).
- 412 [13] A. Bennis, A. M. Lomonosov, Z. H. Shen, and P. Hess, Laser-based mea-
413 surement of elastic and mechanical properties of layered polycrystalline
414 silicon structures with projection masks, *Appl. Phys. Lett.* **88**, 101915
415 (2006).
- 416 [14] A. A. Maznev and A. G. Every, Surface acoustic waves with negative
417 group velocity in a thin film structure on silicon, *Appl. Phys. Lett.* **95**,
418 011903 (2009).
- 419 [15] C. Grünsteidl, I. A. Veres, J. Roither, P. Burgholzer, T. W. Murray, and
420 T. Berer, Spatial and temporal frequency domain laser-ultrasound ap-
421 plied in the direct measurement of dispersion relations of surface acoustic
422 waves, *Appl. Phys. Lett.* **102**, 011103 (2013).

- 423 [16] F. Reverdy and B. Audoin, Elastic constants determination of
424 anisotropic materials from phase velocities of acoustic waves generated
425 and detected by lasers, *J. Acoust. Soc. Am.* **109**, 1965–1972 (2001).
- 426 [17] B. Hosten and B. Castagnede, Optimisation du calcul des constantes
427 élastiques à partir des mesures de vitesses d’une onde ultrasonore, *C. R.
428 Acad. Sc. Paris*, **296**, 297–300 (1983).
- 429 [18] S. Raetz, J. Laurent, T. Dehoux, D. Royer, B. Audoin, and C. Prada,
430 Effect of refracted light distribution on the photoelastic generation of
431 zero-group velocity Lamb modes in optically low-absorbing plates, *J.
432 Acoust. Soc. Am.* **138**, 3522–3530 (2015).
- 433 [19] R. K. Ing and J. Monchalín, Broadband optical detection of ultrasound
434 by two-wave mixing in a photorefractive crystal, *Appl. Phys. Lett.* **59**,
435 3233–3235 (1991).
- 436 [20] B. Campagne, H. Voillaume, L. Gouzerh, and F. Bentouhami, Laser ul-
437 trasonic developments for NDT of aeronautic composite parts, in *13th
438 International Symposium on Nondestructive Characterization of Mate-
439 rials (NDCM-XIII) 2013, Le Mans, France*, volume 19, NDT.net, The
440 e-Journal of Nondestructive Testing & Ultrasonics (2014).
- 441 [21] P. Cawley and C. Theodorakopoulos, The membrane resonance method
442 of non-destructive testing, *J. Sound Vibrat.* **130**, 299–311 (1989).
- 443 [22] I. Solodov, J. Bai, S. Bekgulyan, and G. Busse, A local defect resonance
444 to enhance acoustic wave-defect interaction in ultrasonic nondestructive
445 evaluation, *Appl. Phys. Lett.* **99**, 211911 (2011).

446 List of Figures

447	1	(color online) Illustration of the ZGV Lamb mode generation	
448		using a beam-shaping mask. The generation laser beam is	
449		shaped with periodic slits whose spacing matches the ZGV	
450		wavelength.	6
451	2	(color online) Schematics of the experimental transmission setup.	8
452	3	(color online) The thermoelastic source is a line $4.1 \times 20 \text{ mm}^2$:	
453		(a) time domain and (b) frequency domain B-scans as a func-	
454		tion of the TWM head position. (c) First ZGV peak amplitude	
455		vs. TWM head position: experimental (solid) and theoretical	
456		(dashed) curves.	10
457	4	(color online) Normalized first ZGV peak amplitude vs. TWM	
458		head position when the thermoelastic source is a single line	
459		(solid), multiple lines spaced by λ_{ZGV}^{Al} (dashed) and multiple	
460		lines spaced by $\lambda_{ZGV}^{Al}/2$ (dash-dotted).	11
461	5	(color online) Results obtained in the composite plate with a	
462		thermoelastic source made of three lines: (a) time domain and	
463		(b) frequency domain B-scans vs. TWM head position. (c)	
464		Normalized amplitude of the first ZGV peak vs. TWM head	
465		position (thick line) compared with the result obtained with	
466		a single line source (thin line).	14
467	6	(color online) Composite sample and representation of the scan	
468		lines (solid). Dashed white line circle: maximum size of the	
469		flaw observed optically.	15

470	7	(color online) Time domain B-scans of the composite plate	
471		when the scan line is: line 1 across the impact location (a),	
472		line 2 near the impact location (b), and line 3 far from the	
473		impact location (c). The related frequency domain B-scans	
474		obtained with a Hann time window (respectively d, e and f).	
475		Dashed white lines: maximum dimension of the flaw observed	
476		optically.	16
477	8	(color online) C-scan inspection of the composite plate ob-	
478		tained with the LUCIE system: ratio of the second ultrasonic	
479		echo amplitude to the first ultrasonic echo amplitude	19